

Semi-analytic Shape Function of High-harmonic Electron Cyclotron Emission in Tenuous Plasma

J. Leem,^{1, a)} J. Jo,¹ and G. S. Yun^{1,2}

¹⁾*Department of Physics, Pohang University of Science and Technology, Pohang 37673, Republic of Korea*

²⁾*Division of Advanced Nuclear Engineering, Pohang University of Science and Technology, Pohang 37673, Republic of Korea*

(Dated: 7 July 2021)

Semi-analytic expressions for the electron cyclotron emission (ECE) shape function are developed for arbitrary high harmonics. The integrand of the m^{th} harmonic ECE shape function is fitted with the readily-integrable test function which is parameterized by plasma temperature T_e , harmonic number m and emission angle θ . Semi-analytic formulae for high harmonic ECE emissivity are obtained by integrating the test integrand with the fitting parameters gained from the regression analysis as well as the inductive studies for arbitrary cases. The developed expression matches the numerically-integrated ECE shape function very well and the overall differences between original shape functions and semi-analytic shape functions are evaluated. The expression can be used for rapid analysis of high-harmonic ECE spectra.

PACS numbers: empty

^{a)}juneekleem@gmail.com

I. INTRODUCTION

Electron cyclotron emission (ECE) is an important phenomenon in a magnetized, high-temperature plasma in respect of its applicability in plasma diagnostics. ECE involves useful information such as plasma temperature, density, and energy distribution of electrons¹. More importantly, ECE frequency can be spatially localized when the plasma is subjected to the strong magnetic field² so that the spectroscopic analyses of ECE provide the spatial profiles of plasma properties. In addition to this, the existence of ECE harmonics with their distinct characteristics enriches the plasma information significantly.

The fundamental and the 2nd harmonic of ECE are extensively used for electron temperature diagnostics owing to their optical thickness which enables the usage of black-body radiation³⁻⁵. In contrast, the higher harmonics of ECE, whose optical depths are relatively thin, are potential candidates for the unusual diagnostics such as the measurements of non-Maxwellian(energetic) electrons⁶⁻⁸, and the magnetic fields near the magnetostar⁹. For the diagnostic uses of ECE, the spectral interpretations of the emissivity in various plasma circumstances must be preceded in order to modify the spectra and their corresponding intensities into plasma parameters.

Emissivity $j(\omega)$ is expressed as a multiplication of two components: radiated power per unit solid angle from certain unit plasma volume ($p = \int j(\omega) d\omega$), and a shape function ($\Phi(\omega) = j(\omega)/p$). The analyses of the ECE spectra require a huge number of corresponding shape functions for a given plasma circumstance in order to establish the emission profile¹⁰. However, due to the massiveness of the computing processes as well as the complexities of the ECE shape function formulae, it is inefficient to adjust the numerical approaches on calculating ECE shape functions for a rapid interpretation of the ECE signal. For this reason, the detailed studies and the processes in developing the analytic expressions of the ECE shape functions will be introduced in the next section.¹¹⁻¹³

II. SHAPE OF THE ELECTRON CYCLOTRON EMISSIVITY IN THE FREQUENCY DOMAIN

In magnetized plasma, the electrons gyrate around the magnetic field lines and emit electromagnetic radiations at their fundamental cyclotron frequencies. The harmonic emissions

can be generated when the trajectory of a single electron deviates from the circle, and their actual emission frequencies are broadened and shifted due to the relativistic Doppler effects. The resonance angular frequency $\omega_{m,\text{res}}$ is determined as

$$\omega_{m,\text{res}} = \frac{m\omega_c}{1 - \beta_{\parallel}\cos\theta} \quad (\text{II.1})$$

With $\beta = v_e/c$, $\omega_c = eB_0/\gamma m_e$, $\gamma = \left[1 - (\beta_{\perp}^2 + \beta_{\parallel}^2)\right]^{-1/2}$. The symbols \parallel and \perp represent the parallel and perpendicular components, and θ is the emission angle with respect to the external magnetic field.

In tenuous plasma, the inter-particle interactions are negligible so that the plasma emissivity, which is defined as the radiated power per unit volume, unit solid angle, and unit frequency, can be expressed as a sum of all the radiations from the individual electrons. Detailed derivations of the plasma emissivity for each harmonic radiation are listed in¹, and the expression of normalized spectral emissivity ($\int_0^{\infty} \Phi(\omega) d\omega = 1$, shape function) of 2nd harmonic ECE in local thermal equilibrium (Maxwell distributed electrons) is derived by S. K. Rathgeber¹⁰.

$$\begin{aligned} \Phi_2(\omega; \theta, T_e, B_0) &= \frac{\zeta^{7/2}}{\sqrt{\pi}} \int_{-1}^1 d\beta_{\parallel} \int_0^{\sqrt{1-\beta_{\parallel}^2}} d\beta_{\perp} \beta^5 \\ &\times \delta\left(\left[1 - \beta_{\parallel}\cos\theta\right] \omega - \frac{\omega_{2X}}{\gamma}\right) \exp\left(-\zeta\left[\beta_{\perp}^2 + \beta_{\parallel}^2\right]\right) \end{aligned} \quad (\text{II.2})$$

With $\zeta = m_e c^2 / 2T_e$, $\omega_{2X} = 2eB_0/m_e$. General expression of m^{th} harmonic ECE shape function can be obtained by implementing Rathgeber's idea¹⁰ into m^{th} harmonic emissivity¹

$$\begin{aligned} \Phi_m(\omega; \theta, T_e, B_0) &= \frac{2\zeta^{(2m+3)}}{\sqrt{\pi}m!} \int_{-1}^1 d\beta_{\parallel} \int_0^{\sqrt{1-\beta_{\parallel}^2}} d\beta_{\perp} \beta^{2m+1} \\ &\times \delta\left(\left[1 - \beta_{\parallel}\cos\theta\right] \omega - \frac{\omega_m}{\gamma}\right) \exp\left(-\zeta\left[\beta_{\perp}^2 + \beta_{\parallel}^2\right]\right) \end{aligned} \quad (\text{II.3})$$

Where $\omega_m = meB_0/m_e$ is the cold resonance frequency of m^{th} harmonic ECE. In order to integrate the delta function in (II.3), following identity can be used.

$$\int_a^b f(x)\delta(h(x))dx = \sum_i \frac{f(x_i)}{|h'(x_i)|} \quad (\text{II.4})$$

Where x_i are roots of $h(x)$ in $[a, b]$. Regarding $\gamma = \left[1 - (\beta_{\perp}^2 + \beta_{\parallel}^2)\right]^{-1/2}$, $\beta_{\perp}^2 = 1 - \beta_{\parallel}^2 - (\omega^2/\omega_m^2)(1 - \beta_{\parallel}\cos\theta)^2$ is the only root of the argument of the delta function in (II.3) within

the integration range. Adjusting (II.4) to (II.3) with $\mu = \omega^2/\omega_m^2$.

$$\begin{aligned} \Phi_m(\omega; \theta, T_e, B_0) &= \frac{2\zeta^{(2m+3)/2}\omega}{\sqrt{\pi}m!\omega_m^2} \int_{-1}^1 d\beta_{\parallel} (1 - \beta_{\parallel}\cos\theta) \\ &\times \left[1 - \beta_{\parallel}^2 - \mu(1 - \beta_{\parallel}\cos\theta)^2 \right]^m \exp \left[-\zeta \{ 1 - \mu(1 - \beta_{\parallel}\cos\theta)^2 \} \right] \end{aligned} \quad (\text{II.5})$$

Because β_{\perp} is a real, $\beta_{\perp}^2 = 1 - \beta_{\parallel}^2 - \mu(1 - \beta_{\parallel}\cos\theta)^2 \geq 0$. Thus, the following relation is satisfied with $\eta = 1 + \mu\cos^2\theta$

$$-1 \leq \frac{\mu\cos\theta - \sqrt{1 - \mu\sin^2\theta}}{\eta} \leq \beta_{\parallel} \leq \frac{\mu\cos\theta + \sqrt{1 - \mu\sin^2\theta}}{\eta} \leq 1 \quad (\text{II.6})$$

The integration range of (II.5) is modified as

$$\begin{aligned} \Phi_m(\omega; \theta, T_e, B_0) &= \frac{2\zeta^{(2m+3)/2}\omega}{\sqrt{\pi}m!\omega_m^2} \int_{\beta_{\parallel-}}^{\beta_{\parallel+}} d\beta_{\parallel} (1 - \beta_{\parallel}\cos\theta) \\ &\times \left[1 - \beta_{\parallel}^2 - \mu(1 - \beta_{\parallel}\cos\theta)^2 \right]^m \exp \left[-\zeta \{ 1 - \mu(1 - \beta_{\parallel}\cos\theta)^2 \} \right] \end{aligned} \quad (\text{II.7})$$

Where $\beta_{\parallel\pm} = \left(\mu\cos\theta \pm \sqrt{1 - \mu\sin^2\theta} \right) / \eta$. (II.7) can be simplified by substituting $\alpha = (1 - \beta_{\parallel}\cos\theta)^2$

$$\begin{aligned} \Phi_m(\omega; \theta, T_e, B_0) &= \frac{\zeta^{(2m+3)/2}\omega}{\sqrt{\pi}m!\omega_m^2 \cos\theta} \int_{\alpha_-}^{\alpha_+} d\alpha \\ &\times \left[1 - \left(\frac{1 - \sqrt{\alpha}}{\cos\theta} \right)^2 - \mu\alpha \right]^m \exp \left[-\zeta (1 - \mu\alpha) \right] \end{aligned} \quad (\text{II.8})$$

Where

$$\alpha_{\pm} = \left(\frac{1 \pm \cos\theta \sqrt{1 - \mu\sin^2\theta}}{\eta} \right)^2 \quad (\text{II.9})$$

One may integrate (II.8) m times repeatedly by parts in order to get the analytic expression of m^{th} harmonic ECE shape function. According to the actual work on 2nd X-mode ECE shape function¹⁰, integration by parts becomes increasingly difficult and impractical for higher harmonics though it may not be impossible. Therefore, we studied and developed more practical approach to estimate the shape of the cyclotron emission line including high harmonic emissions.

III. SEMI-ANALYTIC EXPRESSEION OF ECE SHAPE FUNCTION

One of the basic principles of definite integration is that it yields the area under integrand in Cartesian coordinates. Therefore, the practical approach starts with finding the readily

integrable test function which fits into the integrand in the integration range. The integrand $g(\alpha)$ of the generalized shape function in (II.8) is

$$g(\alpha) = \left[1 - \left(\frac{1 - \sqrt{\alpha}}{\cos\theta} \right)^2 - \mu\alpha \right]^m \exp[-\zeta(1 - \mu\alpha)] \quad (\text{III.1})$$

The test function can be inferred from the graphical tendency as well as the inflection and the extremums of the original function. In the low α regime, the expression in square bracket dominates the integrand, and exponential function dominates the integrand in the high α regime. Consequently the test function $f(\alpha)$ for the (III.1) is determined as follow.

$$f(\alpha) = A(\alpha - \alpha_+)^k \exp(-B(\alpha - \alpha_+)^2) \quad (\text{III.2})$$

Parameters A and B are derived by matching the extremums of $f(\alpha)$ and $g(\alpha)$.

$$\begin{aligned} A &= \frac{g_{\text{ext}}}{(\alpha_{\text{ext}} - \alpha_+)^k \exp(-B(\alpha_{\text{ext}} - \alpha_+)^2)} \\ B &= \frac{k}{2(\alpha_{\text{ext}} - \alpha_+)^2} \end{aligned} \quad (\text{III.3})$$

In this case, $(\alpha_{\text{ext}}, g_{\text{ext}})$ is assumed to be the extremum of $g(\alpha)$. Because $g'(\alpha_{\text{ext}})$ is zero by definition, α_{ext} is calculated by solving the following equation.

$$\left(\mu + \frac{1}{\cos^2\theta} \right) \alpha_{\text{ext}}^{3/2} - \left(\frac{2}{\cos^2\theta} \right) \alpha_{\text{ext}} + \left(\frac{m}{\zeta} + \frac{m/\zeta\mu + 1}{\cos^2\theta} - 1 \right) \alpha_{\text{ext}}^{1/2} = \frac{m/\zeta\mu}{\cos^2\theta} \quad (\text{III.4})$$

Which is the form of the cubic polynomial¹¹.

$$Q(x) = \eta x^3 - 2x^2 + (m\epsilon\eta + \sin^2\theta)x - m\epsilon = 0 \quad (\text{III.5})$$

Where $x = \sqrt{\alpha}$, $\epsilon = 1/\zeta\mu$, $\eta = 1 + \mu\cos^2\theta$. The cubic polynomial $Q(x)$ has only one real root in $[\alpha_-, \alpha_+]$ and therefore the root is the biggest among the roots of $Q(x)$ (FIG. 1). Hence, the cubic polynomial $Q(x)$ follows the hyperbolic solution for one real root in¹²

$$\begin{aligned} p &= \frac{3\eta(\sin^2\theta + m\epsilon\eta) - 4}{3\eta^2} \\ q &= \frac{9\eta(2\sin^2\theta - m\epsilon\eta) - 16}{27\eta^3} \end{aligned} \quad (\text{III.6})$$

$$\text{if } p < 0, \quad \alpha_{\text{ext}} = \left\{ 2\sqrt{-\frac{p}{3}} \cos \left[\frac{1}{3} \cos^{-1} \left(\frac{3q}{2p} \sqrt{-\frac{3}{p}} \right) \right] + \frac{2}{3\eta} \right\}^2 \quad (\text{III.7})$$

$$\text{else } p \geq 0, \quad \alpha_{\text{ext}} = \left\{ -2\sqrt{\frac{p}{3}} \sinh \left[\frac{1}{3} \sinh^{-1} \left(\frac{3q}{2p} \sqrt{\frac{3}{p}} \right) \right] + \frac{2}{3\eta} \right\}^2$$

Again, the main goal of this work is to establish the test function $f(\alpha)$ as a function of independent variables $(\omega; m, \theta, T_e, B_0)$. Once the evaluation of $(\alpha_{\text{ext}}, g_{\text{ext}})$ is done, the remaining task is to estimate k in (III.2) & (III.3). The Trust-Region algorithm (also known as restricted-step method¹³) is taken as a regression analysis tool to determine the parameter k which is optimized to give the minimum residuals between the test function $f(\alpha)$ and the original integrand $g(\alpha)$ in the integration range $[\alpha_-, \alpha_+]$ (FIG. 2). This implies that for every normalized frequencies μ (FIG. 2) of the effective emissivity range (FIG. 6), there exists corresponding parameters $k(\mu)$ such that in order to obtain the shape function with high frequency resolution, the semi-analytic approach consequently converges to the numerical analysis.

Regarding the linear dependence of the parameter k on the harmonic number m (FIG. 3), the linear correlation coefficient $d = m/k$ now replaces the role of the fitting parameter k . Instead of calculating every single corresponding parameters $d(\mu) = m/k(\mu)$, the representative parameter $d_o = m/k_o$ is adopted and will be used in the entire μ range to retain our approach not numerical but semi-analytic. Here, individual effects of plasma temperature T_e , harmonic number m and emission angle θ on the shape function are independently investigated (FIG. 4) to support that implementation of the representative parameter $d_o = m/k_o$ is inductively logical. Overall deviations of $d(\mu; m, \theta, T_e)$ from $d_o(m, \theta, T_e)$ are evaluated through calculating σ_d in (III.8). Here, σ_d is weighted and normalized by the original shape function $\Phi_{m, \text{Ori}}$ to ensure its representativeness in the whole μ range. (FIG. 5)

$$\text{Deviation } \sigma_d(m, \theta, T_e) = \frac{\int d\mu \Phi_{m, \text{Ori}}(\mu; \theta, T_e) |d_o(m, \theta, T_e) - d(\mu; m, \theta, T_e)|}{\int d\mu \Phi_{m, \text{Ori}}(\mu; \theta, T_e) |d_o(m, \theta, T_e)|} \quad (\text{III.8})$$

As a result, the reliability of $d_o(m, \theta, T_e)$ is proved except some marginal cases such as that the plasma temperature is over 5 keV and the harmonic number is sufficiently large.

Now, the semi-analytic formula of the shape function can be expressed as

$$\Phi_m(\omega; \theta, T_e, B_0) = \frac{\zeta^{(2m+3)/2}\omega}{\sqrt{\pi}m!\omega_m^2\cos\theta} \int_{\alpha_-}^{\alpha_+} d\alpha A(\alpha - \alpha_+)^{m/d_o} \exp(-B(\alpha - \alpha_+)^2) \quad (\text{III.9})$$

Substituting $x = B(\alpha - \alpha_+)^2$ & $x_{\pm} = B(\alpha_{\pm} - \alpha_+)^2$,

$$\Phi_m(\omega; \theta, T_e, B_0) = \frac{\zeta^{(2m+3)/2}\omega}{\sqrt{\pi}m!\omega_m^2\cos\theta} \int_{x_-}^0 dx \frac{1}{2} AB^{-(m+d_o)/2d_o} x^{(m-d_o)/2d_o} e^{-x} \quad (\text{III.10})$$

Note that the integrand of (III.9) converges to zero as $\alpha \rightarrow \alpha_-$, thus the integration range $[x_-, 0]$ in (III.10) can be replaced by $[\infty, 0]$ as long as $x = k(\alpha - \alpha_+)^2/2(\alpha_{\text{ext}} - \alpha_+)^2 > 0$. By the definition of Gamma function $\Gamma(z) = \int_0^{\infty} x^{z-1} e^{-x} dx$

$$\Phi_m(\omega; \theta, T_e, B_0) = \frac{\zeta^{(2m+3)/2}\omega}{\sqrt{\pi}m!\omega_m^2\cos\theta} \left| \frac{1}{2} AB^{-(m+d_o)/2d_o} \Gamma\left(\frac{m+d_o}{2d_o}\right) \right| \quad (\text{III.11})$$

Therefore, the final expression of semi-analytic m^{th} harmonic ECE shape function becomes

$$\begin{aligned} \Phi_m(\omega; \theta, T_e, B_0) &= \frac{\zeta^{(2m+3)/2}\omega}{\sqrt{\pi}m!\omega_m^2\cos\theta} \left(\frac{2d_o}{m}\right)^{(m+d_o)/2d_o} \\ &\times \left| g_{\text{ext}}(\alpha_{\text{ext}} - \alpha_+) \exp\left(\frac{m}{2d_o}\right) \Gamma\left(\frac{m+d_o}{2d_o}\right) \right| \end{aligned} \quad (\text{III.12})$$

IV. DETERMINING THE PARAMETERS FOR SEMI-ANALYTIC EXPRESSION

Although the semi-analytic expression for the m^{th} harmonic ECE shape function is established in (III.12), it is still impossible to get the actual values of normalized emissivity without knowing the representative parameter $d_o = m/k_o$. Moreover, even if the representative parameter for a certain plasma and observation condition is determined through the regression analysis, it does not provide the prospect of further information in various circumstances. Consequentially, more comprehensive and inductive studies are significantly important to determine the corresponding representative parameters for the arbitrary cases.

In order to get the insight on how the corresponding representative parameter d_o varies with (m, θ, T_e) , a number of regression analyses are performed between the original ECE shape functions which are numerically calculated and semi-analytic expressions which are calculated by (III.12). The evaluation ranges of (m, θ, T_e) are listed in (TABLE. 1). If the plasma temperature is less than 5 keV, a significant correlation can be found among

(d_o, θ, T_e) (FIG. 7). Thus, the correlation equation can be derived as (IV.1) based on the graphical similarity to Fermi-Dirac distribution.

$$d_o(m; \theta, T_e) = \frac{\alpha}{1 + \beta \{ \gamma T_e^{-1} (\theta - \pi/2) \}} \quad (\text{IV.1})$$

The coefficients α, β, γ are determined from the secondary regression analysis in $\log T_e$ domain (FIG. 8). However, there still exists small m dependences on the coefficients. The rough numbers of α, β, γ with different m are listed in (TABLE. 2), therefore the final expression of the $d_o(m, \theta[\text{rad.}], T_e[\text{eV}])$ becomes,

$$d_o(m, \theta, T_e) = \frac{\alpha_2 + \alpha_1 \log_{10}(T_e)}{1 + \{ \beta_2 + \beta_1 \log_{10}(T_e) \} \{ \gamma_2 T_e^{(\gamma_1 - 1)} (\theta - \pi/2) \}} \quad (\text{IV.2})$$

Finally, the differences between the original ECE shape functions and the semi-analytic results are evaluated using (IV.3) which adds up the whole differences in effective emissivity range of μ (FIG. 9).

$$\text{Error (\%)} = \frac{\int d\mu |\Phi_{m, \text{Ori}}(\mu; \theta, T_e) - \Phi_{m, \text{Test}}(\mu; \theta, T_e)|}{\int d\mu \Phi_{m, \text{Ori}}(\mu; \theta, T_e)} \quad (\text{IV.3})$$

V. CONCLUSION

The semi-analytic expression of m^{th} harmonic ECE shape function has been established with readily integrable function. The fitting parameters of the integrable function are examined in various plasma circumstances, and their resultant differences between the semi-analytic expressions and the numerically calculated ECE shape functions have been evaluated to estimate the applicable boundaries of this work, in particular, on fusion plasma regime. This work can be implemented to high-speed analysis of ECE diagnostics as well as their corresponding synthetic diagnostics^{14?} which are usually utilized for the verification and validation tools.

ACKNOWLEDGMENTS

This work was supported by the National Research Foundation of Korea under grant **No. NRF-2017M1A7A1A03064231** and **BK21+** program.

REFERENCES

- ¹I. H. Hutchinson, “Principles of Plasma Diagnostics,” (Cambridge University Press, 2002) pp. 158–169, 2nd ed.
- ²J. Lee, G. S. Yun, M. J. Choi, J. M. Kwon, Y. M. Jeon, W. Lee, N. C. Luhmann, and H. K. Park, “Nonlinear Interaction of Edge-Localized Modes and Turbulent Eddies in Toroidal Plasma under $n = 1$ Magnetic Perturbation,” *Phys. Rev. Lett.* **117**, 075001 (2016).
- ³M. Bornatici, R. Cano, O. D. Barbieri, and F. Engelmann, “Electron cyclotron emission and absorption in fusion plasmas,” *Nuclear Fusion* **23**, 1153 (1983).
- ⁴M. E. Austin and J. Lohr, “Electron cyclotron emission radiometer upgrade on the DIII-D tokamak,” *Review of Scientific Instruments* **74**, 1457–1459 (2003).
- ⁵M. E. Austin, R. F. Ellis, J. L. Doane, and R. A. James, “Improved operation of the Michelson interferometer electron cyclotron emission diagnostic on DIII-D,” *Review of Scientific Instruments* **68**, 480–483 (1997).
- ⁶P. Woskoboinikow, H. C. Praddaude, I. S. FaIconer, and W. J. Mulligan, “2nd–5th electron cyclotron harmonic emission from thermal plasmas in Alcator A,” *Applied Physics Letters* **39**, 548–550 (1981).
- ⁷R. F. Ellis, R. A. James, C. J. Lasnier, and T. Casper, “Electron cyclotron emission diagnostics for mirror devices (invited),” *Review of Scientific Instruments* **56**, 891–895 (1985).
- ⁸L. Figini, S. Garavaglia, E. D. L. Luna, D. Farina, P. Platania, A. Simonetto, and C. Sozzi, “Measure of electron cyclotron emission at multiple angles in high Te plasmas of JET,” *Review of Scientific Instruments* **81**, 10D937 (2010).
- ⁹V. Piirola, T. Vornanen, A. Berdyugin, and S. G. V. Coyne, “A High Magnetic Field Intermediate Polar,” *The Astrophysical Journal* **684**, 558 (2008).
- ¹⁰S. K. Rathgeber, L. Barrera, T. Eich, R. Fischer, B. Nold, W. Suttrop, M. Willensdorfer, E. Wolfrum, and the ASDEX Upgrade Team, “Estimation of edge electron temperature profiles via forward modelling of the electron cyclotron radiation transport at ASDEX Upgrade,” *Plasma Physics and Controlled Fusion* **55**, 025004 (2013).
- ¹¹C. Smorynski, “History of Mathematics. A supplement,” (Springer, New York, NY, 2008) pp. 147–174.

- ¹²G. C. Holmes, “The use of hyperbolic cosines in solving cubic polynomials,” *The Mathematical Gazette* **86**, 473–477 (2002).
- ¹³R. H. Byrd, R. B. Schnabel, and G. A. Shultz, “A Trust Region Algorithm for Nonlinearly Constrained Optimization,” *SIAM Journal on Numerical Analysis* **24**, 1152–1170 (1987).
- ¹⁴M. Kim, M. J. Choi, J. Lee, G. S. Yun, W. Lee, H. K. Park, C. W. Domier, N. C. L. Jr, X. Q. Xu, and the KSTAR Team, “Comparison of measured 2D ELMs with synthetic images from BOUT++ simulation in KSTAR,” *Nuclear Fusion* **54**, 093004 (2014).

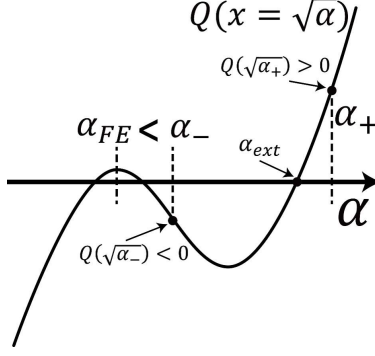


FIG. 1: Overall shape of $Q(x)$ in $\theta \sim 90^\circ$ case. α_{\pm} is in (II.9), and α_{FE} is the first extremum point. $Q(x)$ has three real root in α domain.

Variables	Evaluation range
m	2, 3, 4, 5, 6, 7, 8, 9, 10
θ [$^\circ$]	10, 20, 30, 40, 50, 60, 65, 70, 75, 80, 81 82, 83, 84, 85, 86, 87, 88, 89, 89.9
T_e [eV]	100, 200, 400, 800, 1600, 3200, 6400, 12800

TABLE I: The evaluation ranges of (m, θ, T_e) for the further analysis in this section. Common values in the fusion plasma circumstance are emphasized in red.

m	α_1 [10^{-3}]	α_2	β_1 [10^{-2}]	β_2	γ_1	γ_2
2	-6.38	2.603	-3.740	2.381	0.484	1333.46
3	-6.41	2.393	-1.918	1.851	0.481	1130.80
4	-6.92	2.292	-1.385	1.610	0.476	1014.08
5	-8.41	2.235	-1.227	1.475	0.472	934.33
6	-10.33	2.201	-1.220	1.390	0.468	876.43
7	-11.32	2.175	-1.283	1.332	0.462	839.41
8	-11.93	2.156	-1.390	1.291	0.456	815.36
9	-13.81	2.144	-1.533	1.260	0.451	792.24
10	-17.12	2.141	-1.700	1.238	0.447	767.26

TABLE II: Exact values of α, β, γ with different m . One can use the given values to evaluate the ECE spectrum.

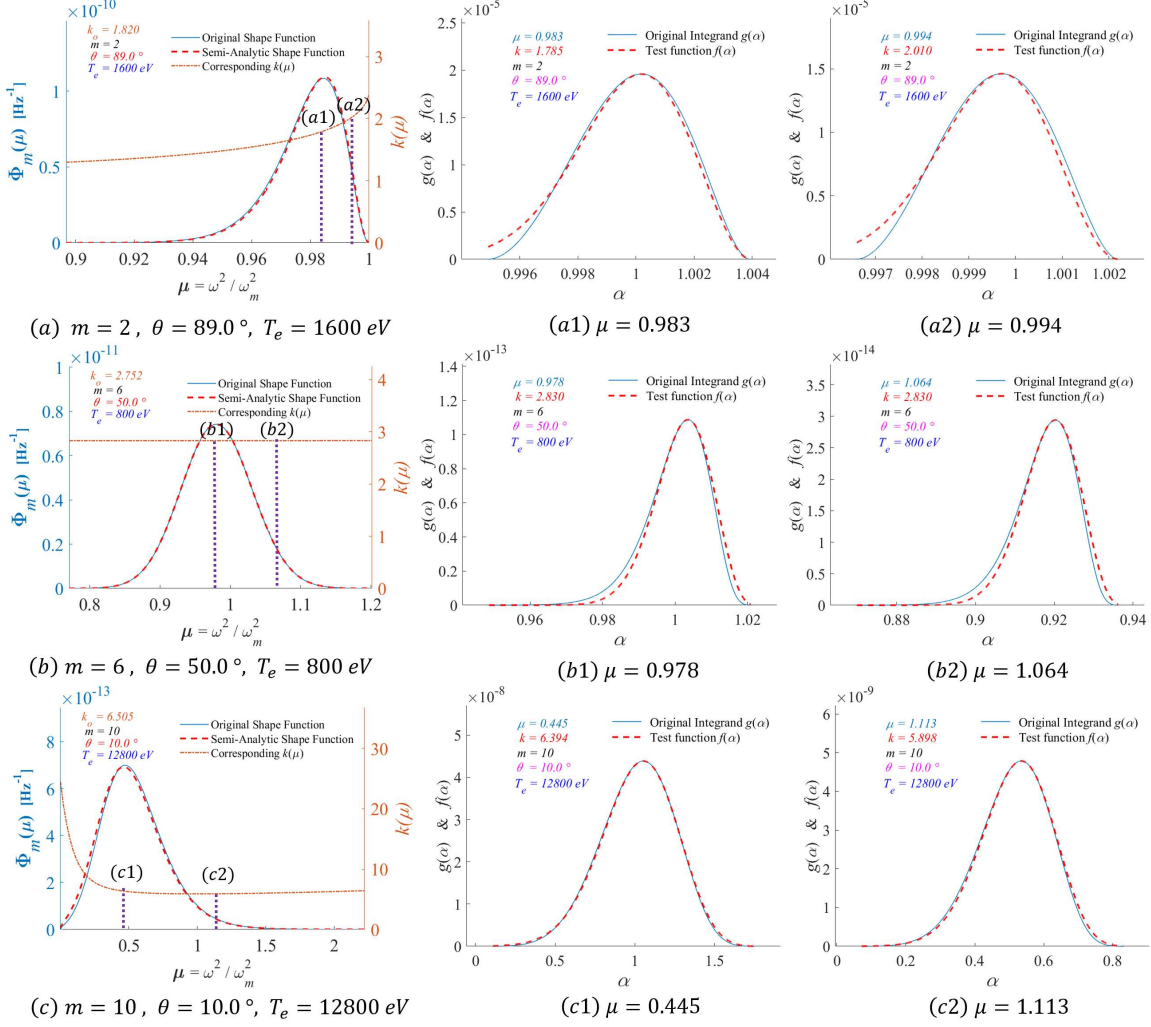


FIG. 2: Original shape functions and their corresponding test functions are plotted by using the representative parameter k_o which is obtained from the regression analysis. Subplot show how the test function $f(\alpha)$ is fitted to the original integrand $g(\alpha)$ for a certain μ . In most cases, k is almost constant for whole effective μ range as in (b), but (a) and (c) show two exceptional cases.

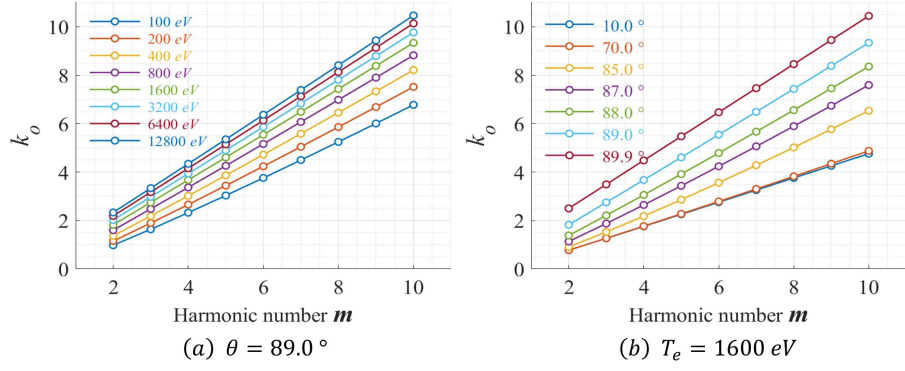


FIG. 3: Linear correlation between harmonic number m and k_o . This implies that the k_o can be replaced by $d_o = m/k_o$

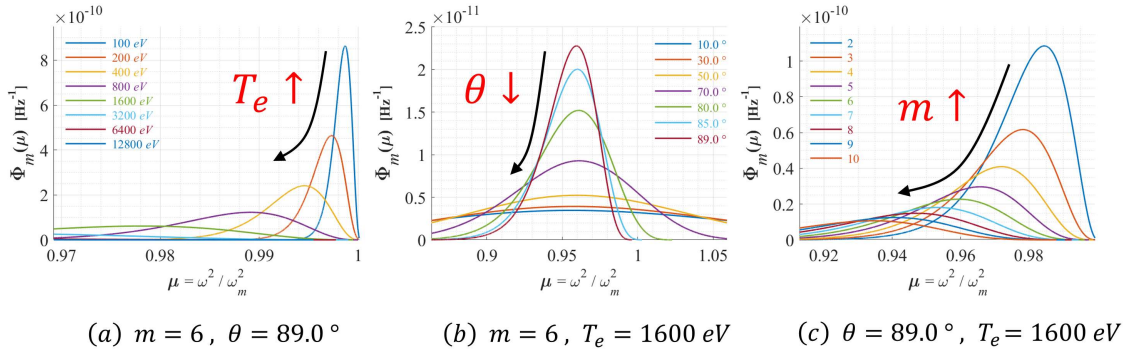


FIG. 4: Individual effects of plasma temperature T_e , harmonic number m and emission angle θ on the shape function.

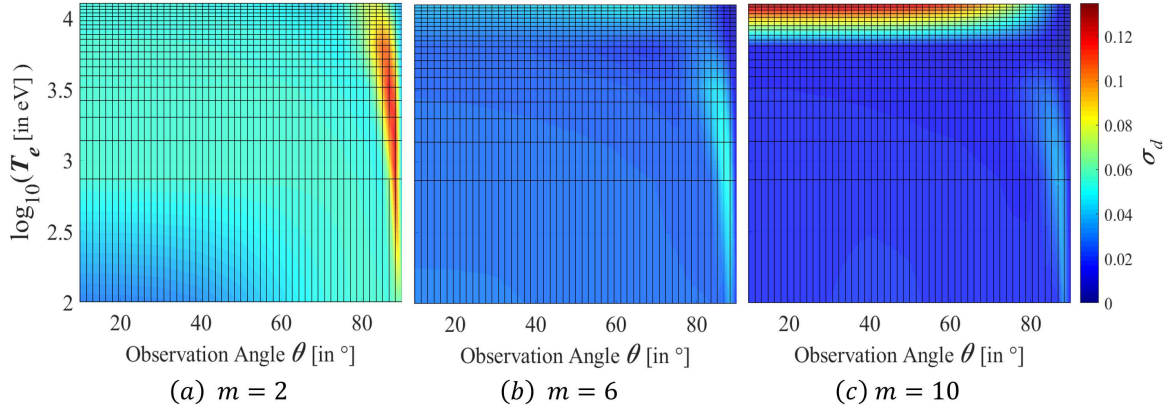


FIG. 5: Plasma temperature T_e , harmonic number m and emission angle θ effects on the Deviation σ_d . Overall deviations do not exceed **0.15** even in the worst cases. This results inductively certificate the usage of $d_o(m, \theta, T_e)$

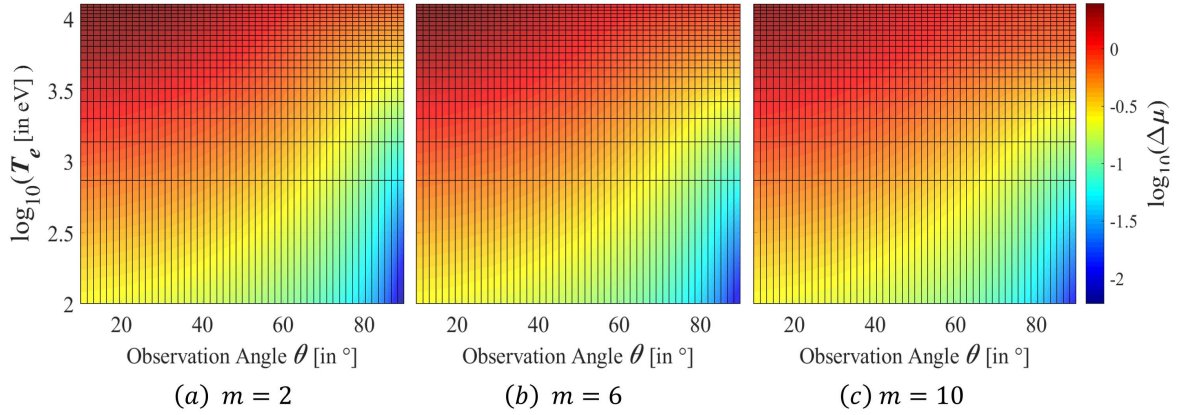


FIG. 6: Doppler broadening effects of the shape function at a glance. Effective emissivity range $\Delta\mu$ is broadened as θ goes 0° and T_e increases.

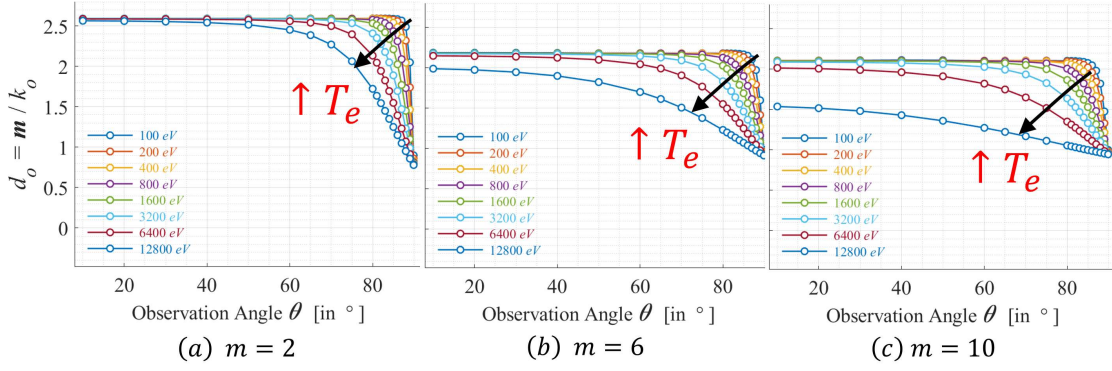


FIG. 7: T_e dependence of d_0 in various m . This correlation has a similarity to Fermi-Dirac distribution.

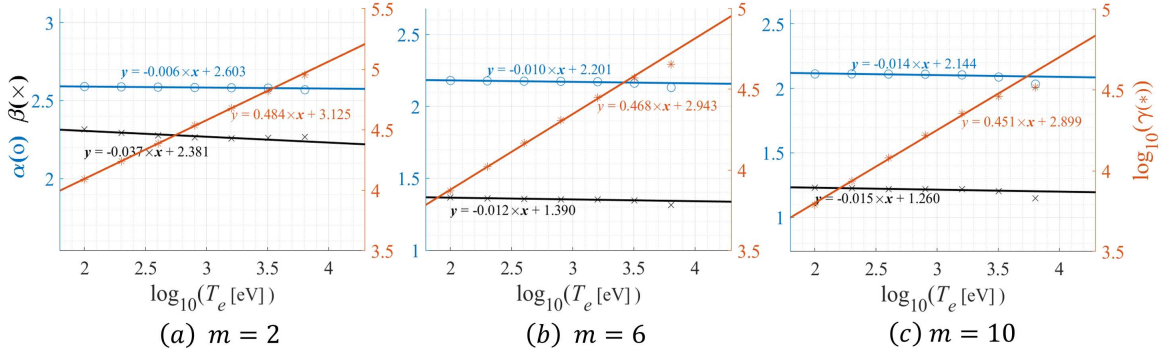


FIG. 8: Individual coefficients in (IV.1) are obtained through the regression analysis with linear fitting.

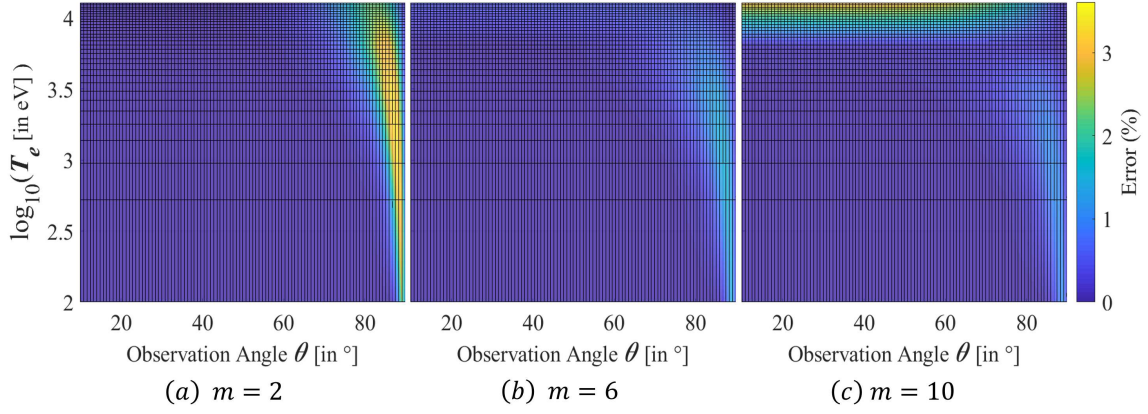


FIG. 9: Overall difference [Error (%)] between the original shape function and the semi-analytic expression is no larger than 4%. There is a close resemblance to Deviation σ_d in (FIG. 5)